Title

Dynamic secretome of bone marrow-derived stromal cells reveals a cardioprotective biochemical cocktail.

Journal

Proceedings of the National Academy of Sciences, 116(28)

Authors

Ellison, David
Suhail, Yasir
Afzal, Junaid
et al.

Publication Date

2019-07-09

DOI

10.1073/pnas.1902598116

Peer reviewed

Dynamic secretome of bone marrow-derived stromal cells reveals a cardioprotective biochemical cocktail

Kshitiz[a,b,1,2], David D. Ellison[c,1], Yasir Suhail[b,1], Junaid Afzal[d], Laura Woo[c], Onur Kilic[a], Jeffrey Spees[e], and Andre Levchenko[a,2]

[a]Yale Institute of Systems Biology, Yale University, West Haven, CT 06516; [b]Department of Biomedical Engineering, University of Connecticut Health Center, Farmington, CT 06030; [c]Department of Medicine, The Johns Hopkins School of Medicine, Baltimore, MD 21205; [d]Department of Cardiology, University of California, San Francisco, CA 94115; and [e]Department of Cellular Molecular and Biomedical Sciences, University of Vermont, Burlington, VT 05405

Edited by Stanislav Y. Shvartsman, Princeton University, Princeton, NJ, and accepted by Editorial Board Member James J. Collins June 5, 2019 (received for review February 13, 2019)

Transplanted stromal cells have demonstrated considerable promise as therapeutic agents in diverse disease settings. Paracrine signaling can be an important mediator of these therapeutic effects at the sites of acute or persistent injury and inflammation. As many stromal cell types, including bone marrow-derived stromal cells (BMSCs), display tissue-specific responses, there is a need to explore their secretory dynamics in the context of tissue and injury type. Paracrine signals are not static, and could encode contextual dynamics in the kinetic changes of the concentrations of the secreted ligands. However, precise measurement of dynamic and context-specific cellular secretory signatures, particularly in adherent cells, remains challenging. Here, by creating an experimental and computational analysis platform, we reconstructed dynamic secretory signatures of cells based on a very limited number of time points. By using this approach, we demonstrate that the secretory signatures of CD133-positive BMSCs are uniquely defined by distinct biological contexts, including signals from injured cardiac cells undergoing oxidative stress, characteristic of cardiac infarction. Furthermore, we show that the mixture of recombinant factors reproducing the dynamics of BMSC-generated secretion can mediate a highly effective rescue of cells injured by oxidative stress and an improved cardiac output. These results support the importance of the dynamic multifactorial paracrine signals in mediating remedial effects of stromal stem cells, and pave the way for stem cell-inspired cell-free treatments of cardiac and other injuries.

paracrine signaling | secretome | secretion dynamics | paracrine dynamics | cell–cell communication

Secreted diffusive molecular factors are critical for intercellular communication enabling complex multicellular behaviors (1–3). Not surprisingly, therefore, secretion of various ligands is highly controlled, frequently dynamic in nature, and, like other cellular phenotypes, dependent on the biological context (4, 5). The essential role of paracrine cell–cell communication is illustrated by dependency of different cell types on cells of other cell types for their survival through interchanged growth and survival factors. Paracrine intercommunication between cells through secreted factors are essential in maintaining tissue homeostasis (6, 7). Pro-survival effect may also be exercised more acutely in response to tissue injury or stress. This effect is possibly enabled by circulating adult stem cells, e.g., those derived from the bone marrow stroma, but the mechanisms underlying cell–cell communication in such acute settings remain poorly explored (8–12).

Paracrine signaling underlies the therapeutic potential of adult stem and stromal cells in diverse contexts (13, 14). The pleiotropic nature of cytoprotective function exercised by stem cells in such contexts suggests that stromal cells modulate their secretory signature to elicit specific responses in the targeted injured tissue. For example, CD133-positive bone marrow-derived mesenchymal stromal cells (BMSCs) currently in phase II clinical trials to treat myocardial infarction can also exercise therapeutic effects in many other tissues, e.g., in the brain following stroke, suggesting that the reported benefits are caused by the potential for diverse cellular secretions, each being specific to the particular injury and tissue type (15, 16). Surprisingly, these cells, like other adult stem cell types, do not appear to directly integrate into the damaged tissue, but rather rapidly and completely clear from the site of MI (myocardial infarction) (10, 17, 18). This paradoxical finding has led to an increasing speculation that transient paracrine signaling is the principal mechanism accounting for BMSC function (1), explaining the survival and rescue of target tissues, including the heart (16, 18).

If factors secreted by adult stem and stromal cells can indeed have tissue-protective and therapeutic effects, mimicking their function constitutes a new cell-independent treatment modality. This requires quantitative determination of context-specific dynamic cell secretion profiles. Historically, such measurements have proven challenging, not only because of technical limitations in the analysis of the composition of complex solutions, but also because of the potential for adaptive adjustment of the secretome to the cell microenvironment (19, 20). Furthermore, secreted ligands can display diverse dynamical profiles, e.g., in the form of a sustained release of a molecule, a transient pulse,

Significance

Intercellular communication between cells in tissues is frequently mediated by secreted factors, with rates of secretion frequently varying over time. Stem cells can be recruited and contribute to the reparative process in diverse tissues. How this versatile cytoprotective effect is achieved is not well understood. Here we describe a simple-to-use platform to estimate the dynamics of cellular paracrine signaling in response to a wide range of physiologically relevant perturbations. When injured cardiomyocytes were presented with a cocktail matching the dynamics and dosage of stromal cell-derived secreted factors, we found an improved survival response, suggesting that secretory dynamics can be a key component of therapeutic recombinant cocktails for tissue repair.

Author contributions: K., D.D.E., and A.L. designed research; K. and D.D.E. performed research; K., Y.S., J.A., and O.K. contributed new reagents/analytic tools; K., D.D.E., Y.S., L.W., and J.S. analyzed data; K. and A.L. wrote the paper; and K., Y.S., O.K., and A.L. helped with edits and images.

Conflict of interest statement: A.L., K., D.D.E, Y.S., and J.A. have filed a patent describing the device mentioned in the manuscript. The application number of the patent filing is 15/525328.

This article is a PNAS Direct Submission. S.Y.S. is a guest editor invited by the Editorial Board.

[1]K., D.D.E., and Y.S. contributed equally to this work.

[2]To whom correspondence may be addressed. Email: kshitiz@uchc.edu or andre.levchenko@yale.edu.

This article contains supporting information online at www.pnas.org/lookup/suppl/doi:10.1073/pnas.1902598116/-/DCSupplemental.

Published online June 25, 2019.

or an oscillatory wave (21–24), even under well controlled, steady environmental conditions. However, the primary research focus has been on a more static view of the nature and composition of secreted ligands that can be seen as links in the maps of cellular communication networks (25, 26). Furthermore, technologically, quantitative analysis of complex interacting cellular systems has been limited by the expense of individual assays and frequent scarcity of biological samples (27, 28). The need to amplify weak signals in such widespread assays as ELISA can introduce a tradeoff between increasing detection sensitivity and absolute quantification (29, 30), whereas direct, nonamplifying fluorescence-based sandwich immunoassays, although more precise and scalable, suffer from limited detection capabilities (31). Advanced mass spectrometric techniques like DESI (desorption electrospray ionization) and LESA (liquid extraction surface analysis) mass spectrometry can measure proteins adsorbed onto a surface in small quantities (32, 33). Microfluidics can provide 2 important advantages in the analysis of cell secretome: (*i*) small volume limiting dilution of the secreted compounds and (*ii*) more predictable liquid handling (34, 35). Recently, these advantages have been used to enable quantifiable measurements of cell secretions down to a single-cell level (36–40). However, important challenges remain. As the cell secretion is measured in the same compartment in which cells are cultured, it is difficult to define the time point at which the secretion of a particular ligand is initiated, compromising the ability of these platforms to yield kinetically resolved secretion profile data (31). This problem is particularly acute for adherent cells, which could have a very different secretory behavior during transient cell adhesion following introduction into the device vs. the more relevant response of fully adhered cells (31, 36). Current devices also have limited ability to precisely evaluate the response to an experimental stimulus delivered within the device, as the secretion and its detection before and after the stimulus may not be time-resolved and separated (41). These limitations are, however, specific to the individual detection platform, which may not be focused on dynamical measurement and can thus be overcome with appropriate modifications.

A more precise analysis of dynamic secretomes could be enabled if an economical use of the biological samples (reflected in relatively few time-resolved measurements) could be coupled with a well-justified reconstruction and interpolation of the concentrations of the secreted ligands in time intervals between the measurements. Arguably, the information required for this interpolation could be recovered from spatial distributions of diffusing compounds, relying on the intimate connection between space and time in diffusion-mediated transport. Frequently, this information is consciously removed in the design of the measurement devices, aimed at achieving "well-mixed" conditions leading to a rapid equilibration of secreted ligands between distinct detection locations within a device (37, 39). However, if this requirement is relaxed and the spatial profiles of secreted ligands are evaluated at each time point, further information can be mined from each experimental measurement, as demonstrated in this study.

Here, we sought to measure secretory dynamics of BMSCs in diverse conditions mimicking those of cardiac reperfusion injury by creating a platform combining microfluidics and protein microprinting with a unique geometry. We took advantage of the measurement of the diffusion-mediated spatial profiles of ligands secreted by BMSCs to reconstruct the temporal dynamics of the detected constituents of the secretome. Our data suggest that cellular secretion profiles, including those produced by BMSCs, can constitute a unique stimulus-matched signature that can strongly affect other cell types and modulate their behavior, e.g., increasing their survival. Furthermore, we also demonstrate antiapoptotic effect of the secretome of BMSCs triggered in response to signals from cardiac cells injured by oxidative stress. Strikingly, this apoptotic effect is retained if the secreted mixture is dynamically mimicked by a mixture of recombinant factors in a cell-free manner, paving the way for new therapeutic methods for rescuing cardiomyocytes from ischemia reperfusion-mediated cell death during cardiac infarction.

Results

A Measurement Platform Using Spatial Information to Reconstruct the Secretion Dynamics. If a dynamically secreted substance diffuses over substantial distances and if the resulting spatial concentration profiles can be assessed, the spatial distribution of the substance can reflect the temporal secretion dynamics (Fig. 1 *A* and *B*). Mathematically, the recovery of this information is an inverse problem of reconstructing the dynamics of the source of the signal from the resulting distribution of the signal concentration at different distances from the source. For instance, if a signal is secreted as a pulse, the resulting wave of increased signal concentration can be detected at time t only up to the distance of approximately $\sqrt{Dt}$ from the source, where D is the diffusion coefficient. Beyond this distance, the signal would have limited effect. Therefore, if a detection mechanism would consist of an array of signal-integrating local microspots, located at different distances from the source, one could establish the timing of the pulse from the distance the wave has traveled by the time of detection, thus reconstructing the signaling kinetics throughout the detection time period even from a single measurement (Fig. 1*B*). More complex signal secretion dynamics can be represented as a collection of pulses, leading to convolution of waves arising from these "elementary pulses" at different distances over time. The inverse problem of reconstruction of the signaling dynamics from the resulting spatial profile can still be solved even for such more complex cases, as demonstrated in *SI Appendix*, Supplementary Information 1, Fig. 1*C*, and *SI Appendix*, Fig. S1. This provides one with the opportunity to rely on a limited number of time-resolved measurements by using arrays of signal detectors located at various distances from the secreting cells. This consideration was the key factor driving the design of an assay described later.

The method we termed "microfluidic fluorescence-linked immunoabsorbent assay" (μFLISA) was implemented in a device with 2 chambers initially fluidically separated by surface tension at the liquid–air interface enabled by closely positioned microfabricated colonnade of pillars (Fig. 1 *D–F* and *SI Appendix*, Fig. S2*A*) (42). Before initiation of detection, the fluidically isolated experimental chamber is seeded with cells of interest (e.g., human BMSCs explored here), which are allowed to adhere and spread and then be subjected to the desired experimental conditions. These experimental conditions can include constant or dynamic administration of a drug- or a cell-specific ligand, change in oxygen tension or acidity, different cell adhesion substratum coating and mechanics, or a medium conditioned by incubation of another cell type. To facilitate reconstruction of paracrine dynamics, the initially fluidically isolated detection chamber contains rows of immobilized microspots of printed antibodies capable of binding a predefined set of secreted ligands diffusing from the experimental chamber. Each row contains multiple spots of the same antibody type, allowing detection of the same secreted factor at different distances from the secreting cells. As the cell culture medium in the experimental chamber can be refreshed before initiation of detection, the detection can be limited only to the compounds that are secreted after a predefined detection initiation point, eliminating the potentially confounding effects of any secretions occurring during cell spreading and preconditioning. The detection is initiated at a desired time point by establishing the fluidic connection between the experimental and detection chambers by increasing hydrostatic pressure using a syringe pump to overcome the surface tension-mediated chamber decoupling (*SI Appendix*, Fig. S2*A*). The detection can then be accomplished by stopping the experiment at desired times and using secondary antibodies to detect the ligands captured at microspots in the

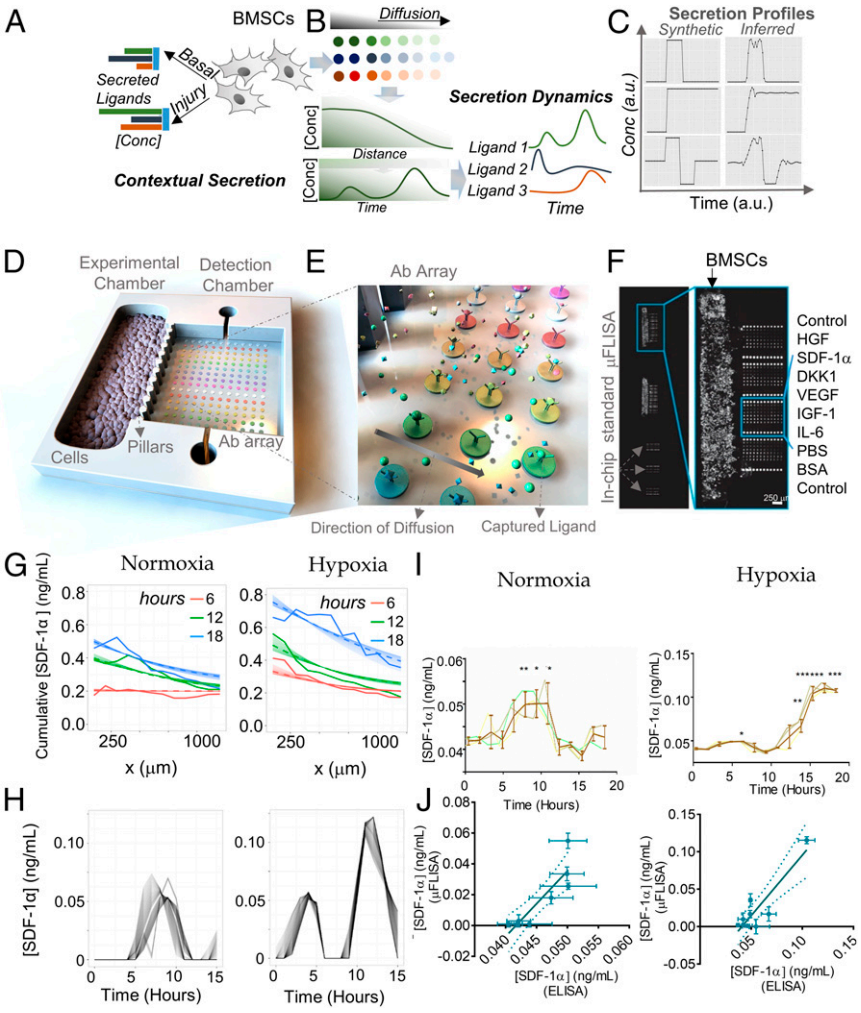

Fig. 1. Quantitative evaluation of secreted factors using μFLISA leads to reconstruction of secretion dynamics in diverse biological conditions. (*A*) Schematic illustration showing that paracrine secretion of BMSCs (bone marrow-derived stromal cells) and other cell types is contextual. Schematically shown are the expected differences in concentrations of different ligands secreted by BMSCs in basal conditions and in response to injury signals from adjacent tissue; the composition of the secretome forms a unique paracrine signature in response to specific biological stimuli. (*B*) Constituents of cellular secretion in tissues or a measurement device could display secretion dynamics reflected in dynamically changing concentration gradient formed by diffusion in surrounding space. These can be integrated by neighboring cells in tissue or capture antibodies in a device at different distances from the secreting cells, such as BMSCs. The measured spatial gradients could be used to reconstruct the original dynamics of secretion for each molecule. (*C*) Initial test of an algorithm to reconstruct the dynamic secretion profiles from spatially graded distribution of ligands. (*D*) A schematic diagram showing the layout of the experimental platform enabling the μFLISA method. The cells are cultured in the experimental chamber initially fluidically isolated from the detection chamber containing rows of microspotted capture antibodies for a subsequent on-chip detection of secreted ligands; the magnified schematic diagram of detection is shown in *E*. (*F*) A micrograph showing the macrofabricated μFLISA platform with cultured BMSCs in the experimental chamber and antibody arrays in the detection chamber after the chambers were allowed to make fluidic contact and the cell secretions detected; note the spatially graded nature of the detected signals. The device contains 2 replicas of such 2-chamber arrangements and an area for the on-chip calibration (see text for details). The device is shown (*Left*) along with a magnified zone with the experimental chamber with cells stained with DAPI and the detection chamber with stained microspots (*Right*). (*G* and *H*) Measured graded distributions (*G*) and reconstructed secretion kinetics (*H*) of SDF1α secreted by BMSCs in normoxia and hypoxia. The secretion kinetics (*H*) are shown as multiple overlaid curves reflecting the experimental uncertainty of the measurements. Each of these curves is in turn used to generate 3 spatial distribution profiles for different time points corresponding to the experimental measurements, overlaid on the experimental data for 6 h (red), 12 h (green), and 18 h (blue) after the start of the experiment for SDF-1α. At least 6 technical replicates for each of the 3 biological samples were measured. SSE values are 0.099 $(ng/mL)^2$ for hypoxia and 0.054 $(ng/mL)^2$ for normoxia. (*I*) Time-course analysis of secreted SDF-1α secretion from BMSCs measured by ELISA in normoxia and hypoxia ($n = 3$ samples). (*J*) Correlation between time-course measurements of SDF-1α secretion from BMSCs by ELISA and μFLISA methods for hypoxia (*Left*) and normoxia (*Right*). Solid lines show the linear regression with $R^2 = 0.81$ for hypoxia and $R^2 = 0.79$ for normoxia; 95% CI shown between dotted lines (*$P < 0.05$, **$P < 0.01$, and ***$P < 0.001$, Student's *t* test). Error bars show SEM.

experimental chamber. The finite element simulations executed in COMSOL to model diffusion of proteins (39, 40) in the device confirmed that diffusion of proteins with the characteristic sizes matching those of the factors examined here is not distorted by pillars separating the chambers, with the diffusion profiles stable over prolonged time periods (*SI Appendix*, Fig. S2*B*). This analysis also predicted that the gradients of secreted ligands in the detection chamber would persist for multiple hours, suggesting that the distribution of the secreted ligands would not be spatially uniform (*SI Appendix*, Fig. S2*C*). Finally, the device contained additional rows of antibody spots in a separate standardization chamber used to make in-chip standard curves relating the fluorescence intensity to a known ligand concentration (Fig. 1*F* and *SI Appendix*, Fig. S2*D*). In each experiment, we used

3 standardization measurements with recombinant ligands of known concentrations (*SI Appendix*, Fig. S2*E*).

Before use, we characterized the operational limits of detection within the device, focusing on the Damköhler number (Da), which describes the ratio of the reaction and diffusion rates of the molecular species undergoing mass transfer (39, 41, 43, 44). Da << 1 indicates that the device is not reaction-limited (i.e., the diffusing substances are not depleted through binding to the detection microspots) and therefore can be used to measure the secretion dynamics using diffusion as a readout. As an example, for the reported rate of secretion by HGF by BMSCs (45), our analysis revealed that Da remains very low (<0.0001; *SI Appendix*, Fig. S3*A*), and that very low Da values are maintained at all locations in the device for at least 24 h of simulated time (*SI Appendix*, Fig. S3*B*). More generally, Da remains low for wide ranges of experimentally controllable parameters, including the number/density of the antibody molecules in a detection spot (S) and the overall secretion rate of a ligand (n_o), taken to be proportional to the number of cells seeded in the experimental chamber. Saturation of the antibody spots could become a limiting factor, but simulations suggested that, for the experimental procedures followed here, it would take more than 24 h for the microspot most proximal to the experimental chamber to be significantly saturated (50% of maximal), thereby establishing the limit on the duration of detection for the experimental parameters used here (*SI Appendix*, Fig. S3*C*). For more extended experimental measurements, antibody concentration in each spot could be easily increased. The ligand–antibody binding was assumed to be integrated over time, as the rates of dissociation are negligible compared with adsorption. This analysis can be used more generally to determine the operational limits of any device with a diffusive ligand coupled to adsorption-based detection. Details of the analysis are shown in *SI Appendix*, Supplementary Information 2.

Measurement of Dynamic Secretion by Bone Marrow-Derived Stromal Cells. We next experimentally examined the spatial and temporal distributions of ligands secreted in response to different conditions relevant to the ischemia reperfusion injury, in which BMSCs have been reported to show reparative potential (46–48). In particular, we analyzed the substances secreted by BMSCs for the presence of a battery of factors previously implicated as both secreted by these cells and cytoprotective for other cell types (15): Hepatocyte growth factor (HGF), vascular endothelial growth factor (VEGF), insulin-like growth factor (IGF1), Dickkopf-related protein-1 (DKK1), Stem cell-derived factor-1α (SDF-1α), and interleukin-6 (IL-6). For the rest of the study, we focused on these factors as potential mediators of the therapeutic effect associated with these cells. For each experiment, we established the linear detection range using standard curves generated as explained here earlier (see, e.g., *SI Appendix*, Fig. S2*D*). We tested the algorithm described earlier (*SI Appendix*, Supplementary Information 1) for its capability to reconstruct the secretion dynamics of detected factors. To test the limit of the algorithm to detect short-term secretory dynamics, we used the algorithm to reconstruct complex secretory dynamic profiles with differing frequencies, and found that the algorithm reliably reconstructed oscillatory profiles of the time periods <4 h with the current device parameters (*SI Appendix*, Fig. S4 and Supplementary Information 3).

To further support the algorithm validity and determine its applicability to general secretion analysis, we theoretically determined how each subsequent measurement of the spatial profiles can help estimate the dynamics of the secretion (*SI Appendix*, Supplementary Information 4). We calculated the uncertainty of the estimated secretion dynamics and its dependence on the period of oscillation, and found that the uncertainty was higher for shorter oscillation periods, but rapidly decreased as the period increased (*SI Appendix*, Fig. S4*G*). We also found that although the predictive power was much greater for the earlier portions of the reconstructed dynamic secretion curves, each subsequent measurement decreased the uncertainty (variance) for later portions of these curves (*SI Appendix*, Supplementary Information 4). More specifically, for the conditions present in the μFLISA platform, we found that 3 measurements at 6, 12, and 18 h following the initiation of detection could substantially limit the uncertainty of the estimates, providing sufficiently accurate estimate for the first 15 h of the secretion dynamics (*SI Appendix*, Fig. S4*H*).

For the selected experimental conditions, our analysis suggested that secreted factors will create spatial concentration gradients in the detection chamber over periods as long as 20 h. We first tested this prediction by using normoxic and hypoxic (1% oxygen) conditioning, starting at the initiation of detection. Indeed, we observed nonuniform spatial distributions of SDF-1α (Fig. 1 *G* and *H*) and other factors (*SI Appendix*, Fig. S5) at all measurement time points (6, 12, and 18 h) after the onset of hypoxia or normoxia, with these concentrations gradually decreasing as the distance to the secreting cells increased. With time, the graded concentration profiles shifted to higher absolute levels, indicating gradual accumulation of the secreted factors, but still showing no evidence of microspot saturation. This result suggested that this method could indeed be used for measurement of continued, dynamically complex secretion dynamics through analysis of diffusive spread.

We thus applied the algorithm to estimate the detailed secretory profiles of cytoprotective factors SDF-1α, HGF, and DKK1 after BMSCs were continuously subjected to hypoxia or normoxia for the overall secretion durations of 6, 12, or 18 h (Fig. 1 *G* and *H* and *SI Appendix*, Fig. S6). The secretion dynamics were estimated by using the algorithm described here earlier, which included minimization of error between the observed spatial ligand distribution and the predicted spatial ligand distribution resulting from the reconstructed secretion dynamics. The corresponding error was low for the SDF-1α (squared SE [SSE] = 0.099 $[ng/mL]^2$ for hypoxia, 0.054 $[ng/mL]^2$ for normoxia; Fig. 1*H*) and HGF secretions (SSE = 0.035 $[ng/mL]^2$ for hypoxia, 0.061 $[ng/mL]^2$ for normoxia; *SI Appendix*, Fig. S6*A*) and for normoxic DKK1, but was somewhat higher for DKK1 secretion in hypoxia as a result of higher variability, which might have depended on the quality of the antibodies used (SSE = 0.237 $[ng/mL]^2$ for hypoxia, 0.050 $[ng/mL]^2$ for normoxia; *SI Appendix*, Fig. S6*B*). Overall, the detailed reconstructed dynamic secretion profiles revealed pronounced differences between hypoxic and normoxic conditions, suggesting that the absolute accumulated values and the dynamics of cell secretome can be affected in low oxygen. Importantly, the algorithm suggested that BMSCs under hypoxic conditions secreted SDF-1α and HGF in 2 successive pulses, with the first peaking between 0 and 5 h and the second peaking at 10 to 15 h. On the contrary, the secretion of both these factors was delayed in normoxic conditions, with only 1 pulse fully observed over the first 15 h, peaking between 5 and 10 h after initiation of detection. Similar results were obtained for secretion of DKK1, again subject to a somewhat higher experimental variability (*SI Appendix*, Fig. S6).

We sought to validate the results by using independent measurement modalities. First, we measured concentrations of the ligands secreted by BMSCs preconditioned in normoxia and hypoxia for 12 h with flow cytometry by using a protein transport inhibitor monensin and staining BMSCs with the corresponding antibodies. We found the results of flow cytometry measurement to be highly consistent with those of μFLISA, confirming the validity of the method (*SI Appendix*, Fig. S7 *A* and *B*). Second, we found that the experimental datasets were sufficiently rich to allow inference of the values of the diffusion coefficient for each detected molecular species. This was particularly interesting, as analytical estimation of diffusion coefficients is difficult because

they depend on a variety of parameters, including the molecular weight, hydration, viscosity of the medium, temperature, and interaction with other molecular species (49). The family of solutions obtained by varying the values of the diffusion coefficient by 50% around the optimal fit values showed that the predicted kinetics were robust to this parameter variation, presenting consistent data and matching the experimental variability in the spatial profiles of the secreted factors (Fig. 1 *G* and *H* and *SI Appendix*, Fig. S6). This also allowed us to contrast the obtained values with those independently reported in the literature, finding good agreement and thus further validating the procedure (*SI Appendix*, Supplementary Information 5). Finally, to also validate the complex dynamic nature of the secretion profiles, we compared the SDF-1α secretory dynamics measured by μFLISA to that measured by using a commercially available high-sensitivity ELISA. We found that ELISA-based assay, which had to be performed at a much finer time resolution (13 time points) showed very similar dynamics of SDF-1α to that estimated by the μFLISA based on just 3 time points (Fig. 1*I*). We note, however, that the ELISA measurements performed at high temporal resolution were more expensive and time- and material-consuming relative to the μFLISA platform. Kinetically, although greater time was needed for oxygen equilibration in the traditional ELISA analysis vs. μFLISA experiments, thus somewhat delaying the response, traditional ELISA and reconstructed dynamic profiles from the μFLISA experiments consistently revealed pulsatile secretion, with the first and second secretion peaks in hypoxic conditions separated by ∼10 h (Fig. 1*I* and *SI Appendix*, Fig. S7*C*). The amplitudes of responses at different time points as measured by μFLISA and ELISA were also quantitatively highly correlated, providing further validation for the described method of reconstruction of the secretion dynamics (Fig. 1*J*). These results suggested that the μFLISA measurements over a small number of time points could indeed reconstruct detailed dynamic secretion profiles.

BMSC Secretory Signatures Are Specific to Physiological Stimuli. Divergent secretory responses triggered by normoxic vs. hypoxic conditions suggested the ability of BMSCs to modulate the secretion profiles in a manner defined by extracellular conditions. We further tested if other factors usually present in the context of cardiac reperfusion injury could also specifically modulate BMSC secretion. To provide a quick comparison test, we focused on a single time point (12 h), using detection at the most proximal microspot to the experimental chamber for each detected ligand (Fig. 2*A*).

By using normoxic conditions as controls, and contrasting the results with the effects of hypoxia reported here earlier, we found that stimulation with a proinflammatory cytokine Tumor Necrosis Factor-α (TNFα; for 18 h) under normoxic conditions significantly altered the secretion profile (Fig. 2 *B–D*) vs. the hypoxic condition. In particular, whereas preincubation in hypoxic conditions had little effect on secretion of VEGF, the effect of TNFα on secretion of this factor was much more pronounced. On the contrary, whereas the effect of TNFα on secretion of IGF1 was undetectable, it was strongly down-regulated in hypoxia. HGF, IL-6, and, to a lesser degree, SDF-1α were all significantly down-regulated in response to hypoxia but up-regulated in TNFα (Fig. 2 *B–D*). Thus, hypoxia and TNFα exposure, which can both be present at the site of many injuries, can separately have dissimilar effects on BMSC secretion, indicating the ability of the cells to adjust the response to the particular extracellular stimulus.

We next tested the effect of a more complex and specific cardiac injury environment, mimicking the oxidative stress conditions accompanying myocardial infarction and reperfusion. To achieve this, we preincubated BMSCs in a medium conditioned by human induced pluripotent stem cell-derived beating cardiomyocytes (hiPSC-CMs) stressed by pretreatment with hydrogen peroxide. As controls, we also preincubated BMSCs in the media collected from untreated hiPSC-CMs, untreated BMSCs, and unstimulated human cardiac fibroblasts (FBCMRs). μFLISA analysis of BMSCs stimulated by the FBCMR-conditioned medium (Fig. 2*E*) exhibited a secretion profile similar to that produced by the control medium collected from untreated BMSCs (Fig. 2*B*). However, the secretory signature of BMSCs generated in response to the medium conditioned by untreated iPSC-CMs changed drastically, showing no detectable DKK1 levels but significant multifold increases in HGF, VEGF, IGF1, and SDF-1α secretions (Fig. 2*F*). Surprisingly, BMSCs exposed to the medium conditioned by peroxide-treated iPSC-CMs exhibited a less dramatic change in the secretory signature, displaying no detectable VEGF, DKK1, and IL-6, but continuing to have increased levels of HGF and SDF-1α and high levels of IGF1 (Fig. 2*G*). Overall, these results suggested that the secretion profiles of BMSCs can show strong conditional specificity reflective of the nature of the adjacent tissue and

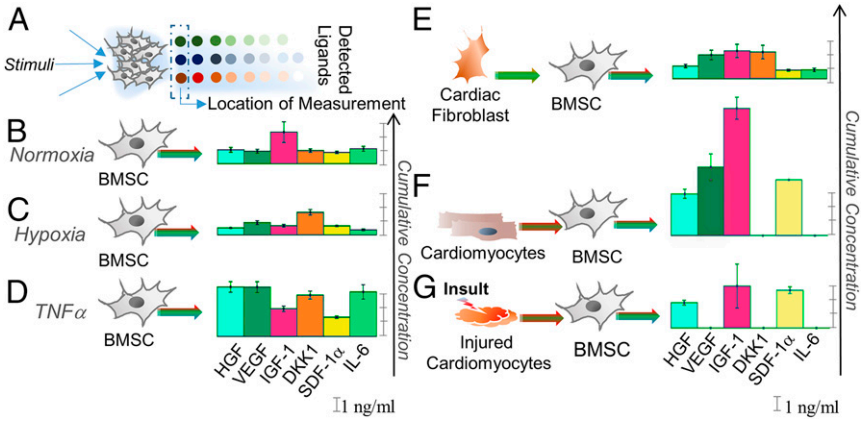

Fig. 2. Secretion of BMSCs is contextual and changes in response to specific environmental signals. (*A*) Schematic illustration showing the measurement of cumulative secretome of BMSCs at the detector microspots most proximal to the experimental chamber, containing cells preconditioned by multiple stimuli. (*B–G*) Cells exhibit distinct and unique secretory signatures reflected by accumulated concentrations of 6 distinct secreted factors corresponding to distinct environmental stimuli: normoxia (*B*), hypoxia (*C*), TNFα (*D*), medium conditioned by cardiac fibroblasts (*E*), medium conditioned by hiPSC-CMs (*F*), and medium conditioned by hiPSC-CMs insulted with peroxide to mimic ischemia reperfusion injury (*G*) (see details in the text). ($n > 6$ biological replicates; n.s. no significance; $^{*}P < 0.05$, $^{**}P < 0.01$, and $^{***}P < 0.001$, Student's *t* test; error bars show SEM.)

the extent of cell stress or damage. Furthermore, they suggested that BMSCs are sensitive to the stress levels of cells, such as cardiac myocytes, and adjust the secreted compounds, perhaps to enable cell-protective effects, a hypothesis we explored in the next set of experiments.

BMSC Secretion in Response to Cardiac Injury Is Cytoprotective. We next attempted to reproduce the cardioprotective effect of the BMSC conditioned media by using a reconstituted mixture of recombinant factors, matching the experimentally determined secretion profiles of BMSCs in response to injured hiPSC-CMs (Fig. 3 *A* and *B*). Strikingly, we indeed found that this mixture had a potent cytoprotective effect closely matching the effect of the BMSC-conditioned medium (Fig. 3*B*). To ascertain whether the combination of factors constituting the mixture increased cytoprotection to a degree greater than any individual component, we measured the extracellular reduction of WST-8 by mitochondrial NADH, which is a correlate of cell metabolic activity and the number of viable cells (17). hiPSC-CMs were treated with hydrogen peroxide after pretreatment with the individual growth factors constituting the mixture (IGF1, HGF, and SDF-1α) or the complete mixture, with the cell viability measured for each pretreatment. Although each component was individually cytoprotective, the application of the mixture resulted in significantly higher cellular viability of hiPSC-CMs vs. any of the individual growth factors (Fig. 3*C*), suggesting a combinatorial

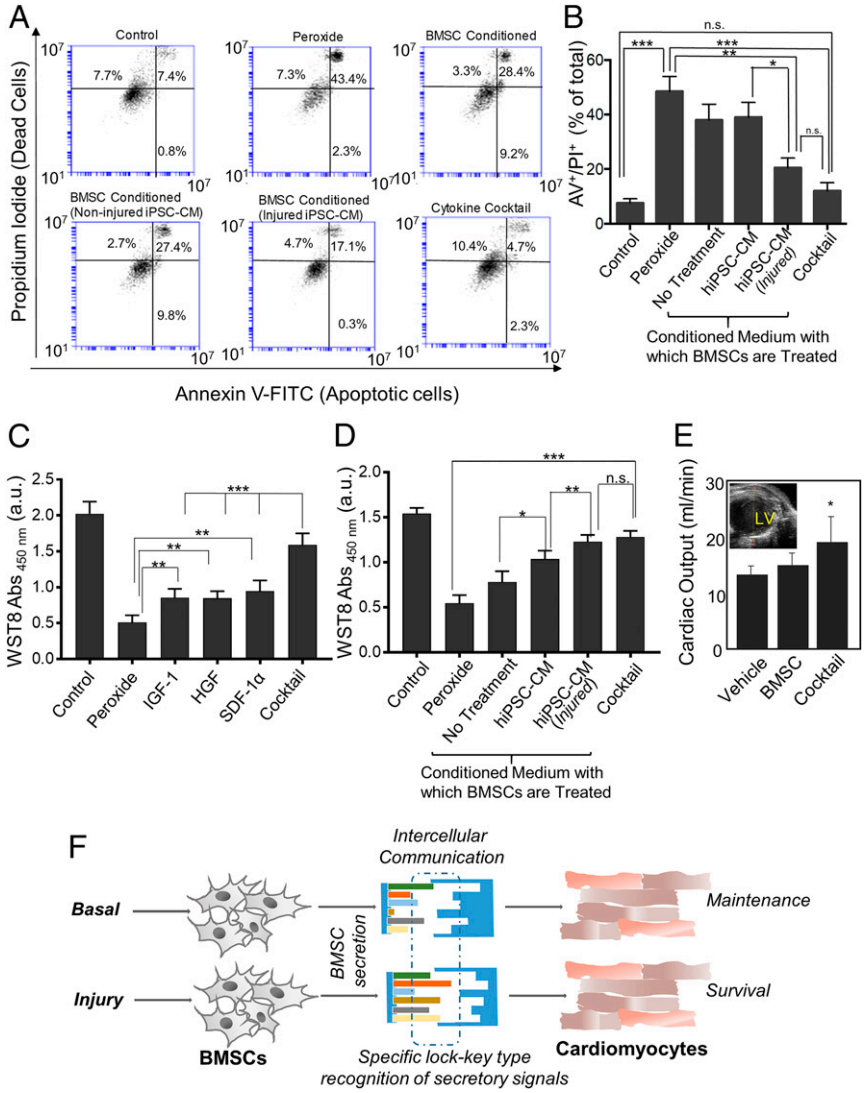

Fig. 3. Mixture of recombinant factors mimicking secretory responses of BMSCs is cytoprotective. (*A*) Flow cytometry dot plots showing Annexin-V and PI staining of hiPSC-CMs treated with the recombinant mixture or media conditioned by BMSCs pretreated as indicated in Fig. 2 *A–F*; the recombinant mixture recapitulates the secretory signature in Fig. 2*G*. (*B*) Quantification of data shown in *A* quantifying cells positive for both Annexin V and PI; dye loading distributions were normal for live and dead cells for all conditions ($n = 4$ biological replicates; error bars show SEM). (*C*) Quantification of hiPSC-CM survival by extracellular reduction of WST-8 following treatment with 500 μM H_2O_2 in the presence of individual factors constituting the mixture or the complete mixture ($n = 6$ biological replicates). (*D*) Quantification of hiPSC-CM survival by extracellular reduction of WST-8 after treatment with 500 μM H_2O_2 following media conditioned as shown in A and B and the biochemical mixture of recombinant factors matching those in B ($n = 8$ biological replicates). (*E*) Cardiac output measured by echocardiography in a mouse model of myocardial infarction injected at the time of reperfusion with PBS solution (vehicle), BMSC-conditioned medium, or the recombinant mixture mimicking BMSC secretion in response to injured hiPSC-CM, along with representative image (*Inset*). (Error bars show SD; n.s., no significance; $*P < 0.05$, $**P < 0.01$, and $***P < 0.001$, Student *t* test.) (*F*) Schematic illustration showing that biological context can define the specific combinations of the factors secreted by stem cells constituting a unique soluble biochemical signature, and this signature is recognized by the target cells to trigger a desired, e.g., cytoprotective, response.

inhibition of peroxide-induced apoptosis. We used the same method to explicitly contrast the cytoprotective effects of the recombinant factors with that of various media conditioned by BMSCs, as explored in Fig. 2. In particular, we collected the medium conditioned by BMSCs, which were themselves pretreated with the media conditioned by uninjured or injured hiPSC-CMs to stimulate cardiac damage specific response. Although both these media displayed cytoprotective effects, the higher rescue from death was observed for the media obtained from BMSCs pretreated with injured cardiac cells (Fig. 3*D*). This rescue effect was closely matched by the effect of the mixture (Fig. 3*D*), indicating that the cytoprotective action of a complex, injury-specific BMSC secretome was closely approximated by a much simpler mixture composition.

We then tested the effect of the mixture in a mouse model of myocardial infarction (detailed in *SI Appendix*, *Methods and Materials*). A total of 100 μL of mixture was injected proximally to the infarcted zone in 3 different locations after ligating the anterior coronary artery. Comparisons were made with control injections (PBS solution) and conditioned medium from BMSCs by echocardiography 3 wk after infarction. We found that the mixture injection resulted in a significant increase of cardiac output (Fig. 3*E*). These results suggested that the battery of factors used in our analysis was indeed characteristic of the cytoprotective effects of the conditioned medium, and that a synthetic mixture composed of the recombinant factors at levels estimated from the secretion analysis can reproduce the cytoprotective effect of BMSCs. Overall, these data indicate that the secretory signature of BMSCs is contextual to the basal or injury signals received from the cardiomyocytes, and that BMSCs can appropriately modulate their secretory response to enable tissue repair (Fig. 3*F*).

Dynamic Mixture Matching the Kinetics of BMSC Secretion Can Further Enhance Cytoprotection. The results described here earlier suggested that even a single time-point measurement of the secreted factors can help design cytoprotective mixtures rescuing peroxide-induced cell death. However, in vivo, the secretion of the factors is likely to be highly dynamic, which might be captured by the μFLISA analyses of cultured cells. We therefore explored the importance of the secretion dynamics vs. the accumulated (or average) values of the abundances of the secreted factors. In particular, we investigated whether the dynamic delivery of the recombinant factors constituting the mixture to the injured myocytes that would match the measured secretion dynamics could further alleviate peroxide-induced stress in hiPSC-CMs. By using our algorithm, we first estimated the secretion dynamics of each individual factor present in the secretion mixture triggered by peroxide-insulted hiPSC-CMs (Fig. 4 *A*–*C*). We then treated the insulted hiPSC-CMs with the medium containing the dynamically varying recombinant factor inputs, matching their time-integrated concentration values to the average values in Fig. 2*G*. The medium was changed every 1 h to recapitulate the estimated dosage dynamics (Fig. 4*D*). We assayed the intracellular reactive oxygen species (ROS) levels as a measure of oxidative stress in hiPSC-CMs after the hydrogen peroxide treatment. We indeed found significantly lower ROS levels following application of the dynamically delivered synthetic mixture vs. the ROS levels in cells exposed to statically delivered mixture (Fig. 4*E*). We next examined the levels of apoptosis in the peroxide-treated cells by using different readouts. First, we found that caspase-3 activity, as measured by hydrolysis of its peptide substrate DEVD, was also significantly lower in dynamically varying mixture conditions (Fig. 4*F*). However, we did not find any significant difference between dynamic and static delivery protocols in the assays relying on the integrity of the plasma membrane as measured by Annexin-V/propidium iodide (PI) assay, suggesting that the primary effect of mixture dynamics was on the control of the caspases and ROS-dependent processes occurring at times earlier than processes leading to membrane disintegration (Fig. 4*G*). Overall, these results strongly imply that not only the average secretion levels, but also the dynamics of cellular secretion, could convey critical cytoprotective signaling information. This result further suggests that precise and absolute measurements of cellular secretions and their dynamics in response to physiologically relevant stimuli can pave the way to cell-free therapy modalities mimicking the effect of adult stem cells.

Discussion

Paracrine signaling by stromal cells is essential for maintaining tissue homeostasis and enabling injury repair, as well as in controlling cancer metastasis. Although the composition of paracrine signals can be measured by the proteomic analysis of the secretome, it is important to further characterize the secretory signature of cells by measuring their contextual secretory dynamics (24). The critical importance of dynamic, context-dependent secretion of a multitude of factors essential for cell function and intercellular communication necessitates inexpensive, high-throughput and quantitative assessment of cellular secretome. Here we describe an analytical platform allowing separation of the preincubation and detection stages of experimental analysis, enabling a more precise analysis of secretion dynamics. We further designed an algorithm permitting extraction of detailed dynamic secretion information from few spatial-temporal distribution datasets. This analysis can be extended to experiments with other adherent and nonadherent cells, enabling considerable amplification of the current analytic capabilities and informing much deeper understanding of cellular interactions. The device could also potentially be combined with state-of-the-art mass spectrometry techniques to obtain broader peptide profile of cell secretion for experimental cross-validation or discovery purposes (32, 50). By using the platform to further characterize the reported secretory signature of bone marrow-derived stromal cells (BMSCs), we found that BMSCs can deliver cytoprotective mixture to injured cardiac cells in response to stimulation by the same injured cells, supporting the hypothesis that the therapeutic effect of BMSCs results from their secretion profiles elicited by the local conditions in an injured tissue. Strikingly, we could recapitulate the cytoprotective effect with dynamically delivered mixture of recombinant proteins, suggesting that detailed and qualitative knowledge provided by the μFLISA platform can suggest new approaches to tissue-specific pharmacological interventions. These findings highlight that secretory dynamics, similar to signaling dynamics (23, 24), could themselves convey specific information about the state of the cell distinctly from the information encoded in the strength of the signal.

Detection of spatially graded concentrations of the secreted factors provided us with the extra information about the secretion dynamics. By using this information in the context of a limited number of measurements, we found that various secreted ligands can exhibit complex, mostly pulsatile secretion dynamics, defined by the environmental inputs. Although it is not unusual to observe or assume pulsatile secretion profiles for hormones, such as insulin (33), the analysis presented here suggests that pulsatile or oscillatory secretion kinetics might extend to many other ligands, including those whose action is local rather than systemic. The advantage of having an oscillatory rather than a persistent stimulation of signaling pathways is currently poorly understood, but we found that this dynamic profile did indeed lead to improved antiapoptotic properties of the recombinant mixture mimicking the cytoprotective effect of BMSCs, suggesting that dynamically variable secretion and thus stimulation of the neighboring cells can be a key feature of the therapeutic effects of the mixture components.

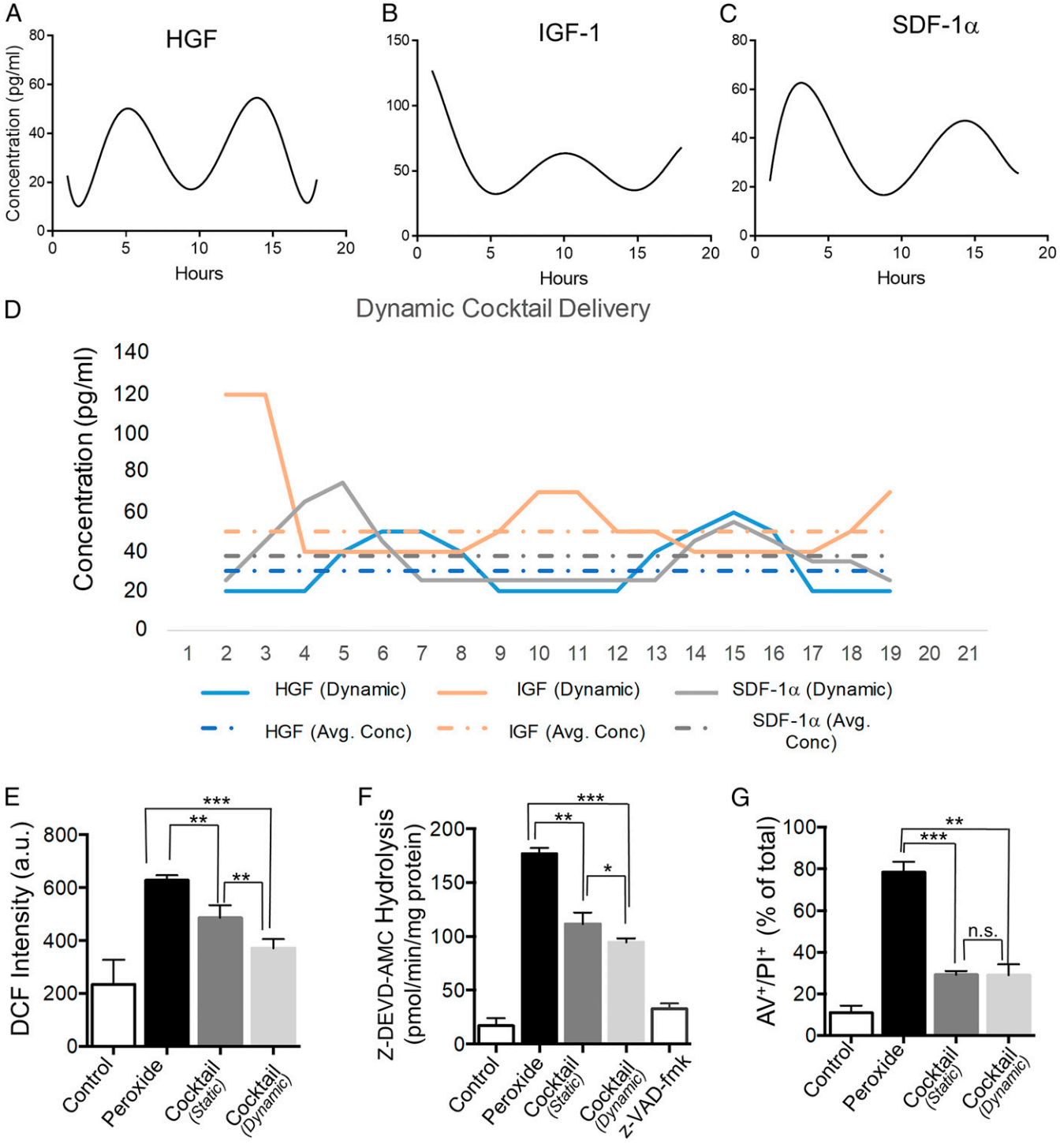

Fig. 4. Matching the kinetics of BMSC secretion enhances cytoprotection of injured cardiomyocytes. Computed kinetics of ligand secretion by BMSCs in response to preconditioning with the medium from injured hiPSC-CMs for (*A*) HGF, (*B*) IGF1, and (*C*) SDF-1α. (*D*) Experimental protocol to match the kinetic dosage of the factors present in the biochemical mixture matched to the average values (dashed lines) used in the static mixture and matched to the computed dynamics in *A*–*C* (solid lines). The concentrations were adjusted every 1 h for 18 h before insulting conditioned hiPSC-CMs with 500 μM peroxide. (*E*) DCF-DA intensity in hiPSC-CMs in the presence of 500 μM H_2O_2 after treatment with the dynamically delivered mixture; untreated cells and cells not conditioned with mixture shown as controls ($n = 4$ replicates with >1,000 cells). (*F*) Caspase-3 activation measured in hiPSC-CMs in the indicated conditions after 30 min of treatment with 500 μM H_2O_2; z-VAD-fmk–treated cells shown as positive control ($n = 3$ biological replicates). (*G*) hiPSC-CM cell death evaluated by Annexin V/PI-based flow cytometry in the presence of 500 μM H_2O_2 after treatment with dynamically delivered mixture; untreated cells and cells not conditioned with mixture shown as controls ($n = 3$ replicates with >10,000 cells; dye loading was normal for subcategories of dead or live cells for all conditions; error bars show SD; n.s. no significance; $^*P < 0.05$, $^{**}P < 0.01$, and $^{***}P < 0.001$, Student *t* test).

Although intuitively appealing, the idea that different ambient conditions can trigger multiple distinct secretory responses, each uniquely fitting these conditions, has not been extensively tested or explored. Our results suggest that the context-specific secretion response is essentially multifactorial. A single secreted component may not be easily used to discriminate between different stimuli. Indeed, we found, for example, that the analysis of secretion of all 6 factors examined here was essential to distinguish between the effects of normoxic conditions vs. a hypoxic environment or of the presence of a proinflammatory cytokine. These results suggest that understanding cell–cell interactions mediated by secreted factors will require a systems-level analysis of the complex secretion signatures not revealed by their simpler components.

Importantly, the context specificity was also observed for the BMSC secretion signatures triggered by healthy vs. injured myocardium, indicating that these adult stem cells can recognize the presence of stress in the adjacent tissue and specifically alter the composition of the secreted factors. These results further suggest the existence of specific signaling factors produced by the insulted cells and signaling mechanisms for detection of these factors in stem cells. It will be of interest to explore the identity of these factors in different tissues and types of tissue stresses, particularly given the ability of BMSCs to exercise therapeutic effect in diverse damaged tissue environments.

The ability to measure and mimic the dynamic cellular secretion providing powerful cytoprotective effects can help pave the way for therapies that are cell-free, but are equally powerful. In the case of cardiac infarction and cardiac ischemia reperfusion, a cell-free therapy consisting only of the recombinant biochemical mixture will not only be more amenable to administration, but also obviate potential side effects of stem cells, including formation of tumors, mistargeting or inadequate tissue homing, and immune rejection (51). Techniques such as μFLISA can allow a systematic determination of stem cell secretions in response to physiologically relevant injury signals, facilitating the creation of cell-free therapy, which would mimic the stem cell secretome in dosage and possibly also in temporal bioavailability.

Materials and Methods

Briefly, we used protein (antibody) microarray printing on an epoxy-coated reactive slide and attached the resulting slide to a prefabricated polydimethylsiloxane (PDMS) microfluidic device aligned in a fashion whereby the antibody array was completely in the detection chamber at a specified distance from the experimental chamber. The experimental chamber is 1.5 mm in width, 150 μm in height, and ∼12.5 mm long, and could allow adherence of approximately 2,000 BMSCs in a monolayer. The colonnade of pillars separating the 2 chambers are 400 μm diagonally, with a gap of 200 μm between them. Cells were introduced into the experimental chamber and allowed to attach and spread before any experimental perturbation was applied. Thereafter, cells were stimulated (as required) and washed with PBS solution to remove residual secreted factors, and both chambers were fluidically connected. The device was immediately sealed off to create a closed system wherein displacement of molecules is primarily through diffusion. After this experiment was completed, the device was disassembled, and the slide was processed to detect capture of antigens in the antibody array. The resultant spatial fluorescent profiles were used as input in the algorithm to estimate the prior temporal profiles of secretion. Further details of study materials and methods are provided in the *SI Appendix*.

ACKNOWLEDGMENTS. This research was supported by the American Heart Association Innovation Grant 16IRG27260356 (to K.) and National Cancer Institute/Cancer Systems Biology Consortium's Research Center Grant 1U54CA209992-01 (to A.L.).

1. A. Abu-Khader *et al*., Paracrine factors released by osteoblasts provide strong platelet engraftment properties. *Stem Cells* **37**, 345–356 (2018).
2. A. K. Shalek *et al*., Single-cell RNA-seq reveals dynamic paracrine control of cellular variation. *Nature* **510**, 363–369 (2014).
3. R. Lugo *et al*., Heterotypic paracrine signaling drives fibroblast senescence and tumor progression of large cell carcinoma of the lung. *Oncotarget* **7**, 82324–82337 (2016).
4. J. Zullo, K. Matsumoto, S. Xavier, B. Ratliff, M. S. Goligorsky, The cell secretome, a mediator of cell-to-cell communication. *Prostaglandins Other Lipid Mediat.* **120**, 17–20 (2015).
5. M. Pavličev *et al*., Single-cell transcriptomics of the human placenta: Inferring the cell communication network of the maternal-fetal interface. *Genome Res.* **27**, 349–361 (2017).
6. X. Zhou *et al*., Circuit design features of a stable two-cell system. *Cell* **172**, 744–757.e17 (2018).
7. E. J. Ruiz, F. Oeztuerk-Winder, J. J. Ventura, A paracrine network regulates the cross-talk between human lung stem cells and the stroma. *Nat. Commun.* **5**, 3175 (2014).
8. F. Arslan *et al*., Mesenchymal stem cell-derived exosomes increase ATP levels, decrease oxidative stress and activate PI3K/Akt pathway to enhance myocardial viability and prevent adverse remodeling after myocardial ischemia/reperfusion injury. *Stem Cell Res.* **10**, 301–312 (2013).
9. M. Gnecchi, Z. Zhang, A. Ni, V. J. Dzau, Paracrine mechanisms in adult stem cell signaling and therapy. *Circ. Res.* **103**, 1204–1219 (2008).
10. I. Chimenti *et al*., Relative roles of direct regeneration versus paracrine effects of human cardiosphere-derived cells transplanted into infarcted mice. *Circ. Res.* **106**, 971–980 (2010).
11. A. M. Hocking, N. S. Gibran, Mesenchymal stem cells: Paracrine signaling and differentiation during cutaneous wound repair. *Exp. Cell Res.* **316**, 2213–2219 (2010).
12. A. Monsel, Y. G. Zhu, V. Gudapati, H. Lim, J. W. Lee, Mesenchymal stem cell derived secretome and extracellular vesicles for acute lung injury and other inflammatory lung diseases. *Expert Opin. Biol. Ther.* **16**, 859–871 (2016).
13. G. D. Kusuma, J. Carthew, R. Lim, J. E. Frith, Effect of the microenvironment on mesenchymal stem cell paracrine signaling: Opportunities to engineer the therapeutic effect. *Stem Cells Dev.* **26**, 617–631 (2017).
14. C. H. Chou, M. Modo, Human neural stem cell-induced endothelial morphogenesis requires autocrine/paracrine and juxtacrine signaling. *Sci. Rep.* **6**, 29029 (2016).
15. B. Bakondi *et al*., CD133 identifies a human bone marrow stem/progenitor cell subpopulation with a repertoire of secreted factors that protect against stroke. *Mol. Ther.* **17**, 1938–1947 (2009).
16. A. Wilkins *et al*., Human bone marrow-derived mesenchymal stem cells secrete brain-derived neurotrophic factor which promotes neuronal survival in vitro. *Stem Cell Res.* **3**, 63–70 (2009).
17. Kshitiz *et al*., Matrix rigidity controls endothelial differentiation and morphogenesis of cardiac precursors. *Sci. Signal.* **5**, ra41 (2012).
18. M. Gnecchi *et al*., Paracrine action accounts for marked protection of ischemic heart by Akt-modified mesenchymal stem cells. *Nat. Med.* **11**, 367–368 (2005).
19. J. M. Duran *et al*., Bone-derived stem cells repair the heart after myocardial infarction through transdifferentiation and paracrine signaling mechanisms. *Circ. Res.* **113**, 539–552 (2013).
20. S. T. Hsiao *et al*., Comparative analysis of paracrine factor expression in human adult mesenchymal stem cells derived from bone marrow, adipose, and dermal tissue. *Stem Cells Dev.* **21**, 2189–2203 (2012).
21. J. Chen *et al*., Kinetics of insulin secretion to acute, repetitive stimulation of islets in vivo in Sprague Dawley rats. *Islets* **2**, 10–17 (2010).
22. S. Ruschen, W. Stellberg, H. Warnatz, Kinetics of cytokine secretion by mononuclear cells of the blood from rheumatoid arthritis patients are different from those of healthy controls. *Clin. Exp. Immunol.* **89**, 32–37 (1992).
23. A. Loewer, E. Batchelor, G. Gaglia, G. Lahav, Basal dynamics of p53 reveal transcriptionally attenuated pulses in cycling cells. *Cell* **142**, 89–100 (2010).
24. J. E. Purvis, G. Lahav, Encoding and decoding cellular information through signaling dynamics. *Cell* **152**, 945–956 (2013).
25. J. A. Ramilowski *et al*., A draft network of ligand-receptor-mediated multicellular signalling in human. *Nat. Commun.* **6**, 7866 (2015).
26. F. H. Biase, K. M. Kimble, Functional signaling and gene regulatory networks between the oocyte and the surrounding cumulus cells. *BMC Genomics* **19**, 351 (2018).
27. J. Cosme, P. P. Liu, A. O. Gramolini, The cardiovascular exosome: Current perspectives and potential. *Proteomics* **13**, 1654–1659 (2013).
28. S. Principe *et al*., Tumor-derived exosomes and microvesicles in head and neck cancer: Implications for tumor biology and biomarker discovery. *Proteomics* **13**, 1608–1623 (2013).
29. S. L. Servoss, R. Gonzalez, S. Varnum, R. C. Zangar, High-throughput analysis of serum antigens using sandwich ELISAs on microarrays. *Methods Mol. Biol.* **520**, 143–150 (2009).
30. C. K. Dixit, S. K. Vashist, B. D. MacCraith, R. O'Kennedy, Multisubstrate-compatible ELISA procedures for rapid and high-sensitivity immunoassays. *Nat. Protoc.* **6**, 439–445 (2011).
31. M. Elitas, K. Brower, Y. Lu, J. J. Chen, R. Fan, A microchip platform for interrogating tumor-macrophage paracrine signaling at the single-cell level. *Lab Chip* **14**, 3582–3588 (2014).
32. W. Rao, A. D. Celiz, D. J. Scurr, M. R. Alexander, D. A. Barrett, Ambient DESI and LESA-MS analysis of proteins adsorbed to a biomaterial surface using in-situ surface tryptic digestion. *J. Am. Soc. Mass Spectrom.* **24**, 1927–1936 (2013).
33. S. S. Basu *et al*., In vitro liquid extraction surface analysis mass spectrometry (ivLESA-MS) for direct metabolic analysis of adherent cells in culture. *Anal. Chem.* **90**, 4987–4991 (2018).
34. Q. Zhou *et al*., On-chip regeneration of aptasensors for monitoring cell secretion. *Lab Chip* **14**, 276–279 (2014).

35. J. P. Wikswo *et al.*, Engineering challenges for instrumenting and controlling integrated organ-on-chip systems. *IEEE Trans. Biomed. Eng.* **60**, 682–690 (2013).
36. K. Tsioris, A. J. Torres, T. B. Douce, J. C. Love, A new toolbox for assessing single cells. *Annu. Rev. Chem. Biomol. Eng.* **5**, 455–477 (2014).
37. A. Kukat, D. Edgar, I. Bratic, P. Maiti, A. Trifunovic, Random mtDNA mutations modulate proliferation capacity in mouse embryonic fibroblasts. *Biochem. Biophys. Res. Commun.* **409**, 394–399 (2011).
38. Y. Lu *et al.*, High-throughput secretomic analysis of single cells to assess functional cellular heterogeneity. *Anal. Chem.* **85**, 2548–2556 (2013).
39. V. A. Adalsteinsson *et al.*, Single cells from human primary colorectal tumors exhibit polyfunctional heterogeneity in secretions of ELR+ CXC chemokines. *Integr. Biol.* **5**, 1272–1281 (2013).
40. Y. J. Yamanaka *et al.*, Cellular barcodes for efficiently profiling single-cell secretory responses by microengraving. *Anal. Chem.* **84**, 10531–10536 (2012).
41. A. J. Torres, A. S. Hill, J. C. Love, Nanowell-based immunoassays for measuring single-cell secretion: Characterization of transport and surface binding. *Anal. Chem.* **86**, 11562–11569 (2014).
42. D. Ellison *et al.*, Cell-cell communication enhances the capacity of cell ensembles to sense shallow gradients during morphogenesis. *Proc. Natl. Acad. Sci. U.S.A.* **113**, E679–E688 (2016).
43. Y. Gao *et al.*, A mathematical method for extracting cell secretion rate from affinity biosensors continuously monitoring cell activity. *Biomicrofluidics* **8**, 021501 (2014).
44. Y. Deng *et al.*, An integrated microfluidic chip system for single-cell secretion profiling of rare circulating tumor cells. *Sci. Rep.* **4**, 7499 (2014).
45. B. Bakondi, I. S. Shimada, B. M. Peterson, J. L. Spees, SDF-1α secreted by human CD133-derived multipotent stromal cells promotes neural progenitor cell survival through CXCR7. *Stem Cells Dev.* **20**, 1021–1029 (2011).
46. J. Wu *et al.*, Intravenously administered bone marrow cells migrate to damaged brain tissue and improve neural function in ischemic rats. *Cell Transplant.* **16**, 993–1005 (2008).
47. W. Lu *et al.*, Mesenchymal stem cells attenuate acute ischemia-reperfusion injury in a rat model. *Exp. Ther. Med.* **10**, 2131–2137 (2015).
48. T. A. Markel, T. D. Crafts, A. R. Jensen, E. B. Hunsberger, M. C. Yoder, Human mesenchymal stromal cells decrease mortality after intestinal ischemia and reperfusion injury. *J. Surg. Res.* **199**, 56–66 (2015).
49. M. E. Young, P. A. Carroad, R. L. Bell, Estimation of diffusion-coefficients of proteins. *Biotechnol. Bioeng.* **22**, 947–955 (1980).
50. C. C. Marasco, J. R. Enders, K. T. Seale, J. A. McLean, J. P. Wikswo, Real-time cellular exometabolome analysis with a microfluidic-mass spectrometry platform. *PLoS One* **10**, e0117685 (2015).
51. C. H. Wang, W. J. Cherng, S. Verma, Drawbacks to stem cell therapy in cardiovascular diseases. *Future Cardiol.* **4**, 399–408 (2008).